The small punch creep test: some results from a numerical model

M. Evans · D. Wang

Abstract Obtaining accurate estimates of remanent creep life is of great importance to the power generating industry. The small punch creep test promises to be a useful way forward in this respect. However, a major concern with the test revolves around the ability to convert small punch test data into the required uniaxial equivalents. Experimental results within the literature have given contradictory results partly due to the large experimental scatter inherent within the test and so this article reports some results from a recently developed stochastic finite element model of the small creep punch test that provides guidance on this matter. The uniqueness of the model is based on its realistic creep deformations laws, including strain hardening, thermal softening and damage accumulation that enables it to produce life predictions for virgin material as well as for material with pre existing damage. It is shown that the model produces excellent life predictions for virgin 0.5Cr–0.5Mo–0.25V steel and for damaged 1.25Cr–1Mo steel over a wide range of test conditions. The model also predicts that the dependency of the time to failure on minimum displacement rates is such that small punch test data can be converted into uniaxial data using relatively simple analytical expressions.

M. Evans (✉)
Materials Research Centre, School of Engineering,
Swansea University, Singleton Park, Swansea SA2 8PP, UK
e-mail: m.evans@swansea.ac.uk

D. Wang
Interdisciplinary Research Centre, Swansea University,
Singleton Park, Swansea SA2 8PP, UK
e-mail: D.Wang@swansea.ac.uk

Notation

$\dot{\xi}_{ij}$	Strain rate tensor
ε_t	Total creep strain at time t (%/100)
ε_f	Elongation at failure (%/100)
$\varepsilon_{\min}$	Minimum creep rate (s^{-1}) from uniaxial tests
$\varepsilon_{d,\min}$	Minimum displacement rate ($mm(s^{-1})$) from small punch test
θ_j	Theta parameter used to describe a creep curve (j = 1, 4)
Θ_i	Natural log of θ_j
$\bar{\Theta}_j$	Mean value for Θ_j
$\hat{\Theta}_{i,j}$	Randomly generated value for Θ_j
$\hat{\theta}_j$	Randomly generated value for θ_j
$\bar{\tau}$	Local Von Mises flow stress
τ_{ij}	Cauchy stress tensor
τ'_{ij}	Deviatoric stress
τ_m	Mean stress
γ_j	Variance of θ_j
ρ_j	Mean variance of Θ_j
σ^*	Normalised stress
σ	Stress (MPa)
$a_{j,0}, b_{j,0}, c_{j,0}, d_{j,0}$	Parameters of the theta interpolation/extrapolation function in the deterministic model
$a_{j,k}, b_{j,k}, c_{j,k}, d_{j,k}$	Parameters of the theta interpolation/extrapolation function for the kth run of the stochastic model
a, b, c, d	Parameters of the failure strain interpolation/extrapolation function in the deterministic model
d	Punch head displacement (mm)
m_k, f_k	Parameters of the critical damage interpolation/extrapolation function for the kth run of the punch test model

r, z	Disc point coordinates
T	Temperature (K)
t_f	Time at failure
U	A randomly drawn number between 0 and 1
$\Phi(U)^{-1}$	A standard normal variate
u_i	Velocity field
V	Velocity
W_{crit}	Continuum damage at failure (dimensionless)
x_1	Punch hole diameter (mm)
x_2	Disc diameter (mm)
x_3	Disc thickness (mm)
x_4	Punch head radius (mm)
x_5	Friction coefficient ($0 \leq x_5 \leq 1$)
x_6	Preexisting damage (dimensionless)
x_7	Load (N)

Introduction

The life assessment and potential for failure of "in-service" components is a critical issue in the safety and reliability of operating power stations which are approaching the end of their design lives. New policies relating to environmental protection and safety at work, together with major advances in analytical techniques for life assessment—which suggest the initial safety factors of these plants were unduly high—have made it more profitable to invest in the modernisation of existing plants rather than in building new ones. However, such modernisation only makes economic sense if existing plants have sufficient residual life and so reducing the uncertainty in evaluating remaining plant life is of primary importance to the power generating industry.

However, traditional tests, such as the uniaxial creep test, are not well suited to this problem. This is because of insufficient material to sample and because the size of the required sample could undermine the structural integrity of the in-service component. The small punch test is an innovative technique based on miniaturised specimens and is a promising solution to this problem. The small punch test was developed at MIT for radiation embrittlement and first reported in 1981 [1]. It was then extensively developed in Japan, particularly at Tohoku University [2]. The first collaborative efforts in small punch test standardisation were reported by the Japanese Atomic Energy Research Institute (JAERI) in 1988 [3]. In the United States, further work by Electric Power Research Institute (EPRI) and Failure Analysis Associates (now Exponent) since the late 1980s [4] led to the introduction of the technique into Europe from 1992 by Swansea University [5] and Electric Research Association (ERA) in the UK and Centro

Elettroecnico Sperimentale Italiano (CISE) in Italy (now CESI) [6, 7].

The small punch test (SP) is a semi-destructive technique because it uses a very limited amount of material, with the specimens being discs of around 0.5 mm thick and around 8–10 mm in diameter. Such small samples taken from components in service not only leave the structural integrity of thick components intact or at least repairable, but allow also for the possibility of focusing on the critical locations of the component (those areas that are more highly stressed and damaged).

Despite these advantages, the power generating industry has been slow to accept the use of this technique. This in part reflects concerns that the reproducibility of the results from such a test is highly dependent upon the geometry of the specimen and the test apparatus. This concern can only be overcome through the development and imposition of a strong code of practice covering both testing and analysis. The other major concern with the technique is that associated with converting the small punch test data into the required uniaxial equivalents. Solutions to these two problems can be sought either through detailed experimentation or through the computer modelling of the small punch creep test.

On the experimental front and in Europe an important push towards such standardisation has come from two main sources. First, between 1994 and 1997 the Copernicus SP project [8] developed a creep small punch test configuration but no code of practice was agreed. Second, between 2000 and 2003, and inside the European Pressure Equipment Research Council (EPERC]), a collaborative project was set up among a few interested parties (CESI in Italy, Joint Research Centre Institute for Energy of the European Community (JRC) in the Netherlands and the University of Swansea in the UK) that consisted of a creep round robin exercise [9]. As a result of that exercise a step towards a real code of practice was made. Over a more recent time span the CEN (one of three European Standardisation organisations recognised by the EC) has been working to produce a code of practice for the small punch creep test. In 2006 they published, as a Workshop Agreement, a CEN code of practice [10]. With regard to test specimen geometry they concluded that test specimens should measure 8 mm in diameter with a thickness of 0.5 mm and these should be tested in an inert argon environment.

A major concern with this experimental approach is that the large scatter known to be present in small punch creep test data would make the identification of a suitable code of practice problematic and inconclusive. To avoid this issue of experimental scatter and so compliment the experimental approach, Evans et al. [11, 12] developed an elastic–viscoplastic finite element model of the punch creep test, written in Salford Fortran, which produces as an

output the displacement time curve up to the point of fracture. The model uses the realistic creep deformation law of Evans [13], which includes strain hardening, thermal softening and damage accumulation. Unlike other finite element models of the small punch creep test (e.g. Hankin et al. [14]), these laws enable the model to be run for any amount of preexisting continuum damage. In the model, the displacement time curve is made a function of the following variables which form the inputs into the model: The hole diameter (x_1), the disc diameter (x_2), the disc thickness (x_3), the punch head radius (x_4), the coefficient of friction (x_5), the preexisting damage present in the disc (x_6) and the punch load (x_7). The model is stochastic in nature in that it has built into it experimentally measured creep variability, so that confidence intervals for the models predictions are also obtainable.

Evans and Wang [15] have made use of the finite element model of the small punch test, together with a response surface methodology, to determine whether there is indeed a specific geometry (and hence a code of practice for testing) that makes the test most useful. That is, maximises the sensitivity of the test to preexisting damage and minimises the sensitivity of the test to the geometry of the specimen and test apparatus. They found that the failure time was most sensitive to disc thickness, hole diameter, initial damage and the punch head radius but least sensitive to disc diameter and load (see Fig. 1 for explanation of the above variables). Under clamping, the optimum specimen geometry was found to be one with a disc diameter of 9.2 mm and a disc thickness of 0.65 mm—both slightly higher than that recommended by CEN. To be acceptable as recommendations, the numerical model used above requires detailed verification.

This article addresses this verification issue and also the second issues raised above concerning the conversion of small punch test data into the required uniaxial equivalents.
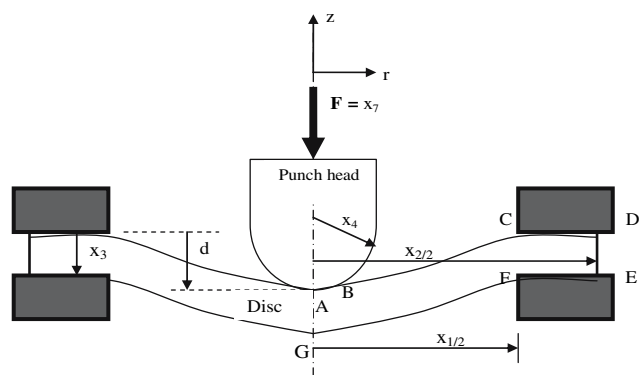

Fig. 1 Schematic of axi-symmetric small punch test (punch hole diameter = x_1, disc diameter = x_2, disc thickness = x_3, punch head radius = x_4, axial load (F) = x_7. ABCDEFG are points on the discs surface. z and r are disc point coordinates

Measurements of minimum displacement rates from the small punch creep test when plotted against time to failure (t_f) frequently show the same type of dependency of t_f on applied stress as observed in uniaxial creep tests, but with a shift along the t_f axis. This shift is different for different materials and different test geometries. The main objective of this article is to develop a better understanding of this shift, its dependence on test parameters and whether it is always parallel in nature. The experimental approach to this problem has proved to be rather inconclusive with some studies (e.g. Stratford *et. al.* [16]) showing minimum displacement rates (from the punch test) and minimum creep rates (from uniaxial tests) sitting on parallel lines when plotted against t_f on a log–log scale, while other studies have shown them to sit on nonparallel lines (e.g. National Physical Laboratory [17]). This article therefore takes the alternative approach of using the results from a finite element model of the small punch creep test to help resolve this issue.

To meet this objective the article is structured as follows. The next section briefly discusses the materials tested for this article. The following section provides a quick overview of the small punch creep test model. This is followed by a results section that is split into two parts. The first part verifies the punch test model using both virgin 0.5Cr–0.5Mo–0.25V steel and pre-damaged 1.25Cr–0.5Mo steel. The second part shows the Monkman–Grant type results obtained from the model for 0.5Cr–0.5Mo–0.25V steel and compares these to some uniaxial experimental data. The final section concludes with recommendations for future work.

The materials

The uniaxial creep testing on 0.5Cr–0.5Mo–0.25V was carried out in the creep laboratories at the Interdisciplinary Research Centre (Swansea) as part of a research programme financed by the Engineering & Physical Science Research Council and the Central Electricity Generating Board in 1983. This was short-term accelerated constant stress creep testing. All the tests were carried out in an air atmosphere. The 0.5Cr–0.5Mo–0.25V material, supplied by CEGB, consisted of fabricated header pipe and its chemical composition (in wt.%) is shown in Table 1. Following the standard heat treatment (10 h at 1,238 K, 15 h 973 K and 15 h at 933 K) for this material, it had a yield stress of 263 MPa at 808 K and a yield stress of 191 MPa at 868 K. This data has appeared extensively in the literature since it was first published by Evans et al. [18].

Twenty-two test pieces, with gauge lengths of 28 mm and diameters of 5 mm, were tested in tension over a range

Table 1 Chemical analysis of test material in wt.%

Chemistry (%)	C	Si	Mn	Cr	M_0	Ni	Cu	Sn	S	P	V
0.5Cr–0.5Mo–0.25V	0.12	0.26	0.58	0.34	0.66	0.2	–	–	0.019	0.0009	0.26
1.25Cr–0.5Mo	0.16	0.56	0.35	1.29	0.44	0.07	–	–	0.005	0.007	–

of stresses at 808, 838, 868 and 913 K using high-precision constant-stress machines. At 808 K, five specimens were placed on test over the stress range 250–350 MPa, at 838 K eight specimens were placed on test over the stress range 175–310 MPa, at 868 K six specimens were tested over the stress range 160–250 MPa and at 913 K three specimens were tested over the stress range 128–200 MPa. The longest recorded failure time was 1,471 h. Up to 400 creep strain/time readings were taken during each of these tests and normal creep curves were observed under all these test conditions.

The 1.25Cr–0.5Mo material was supplied by Ontario Hydro, Canada, and was taken from new thick wall seamless pipe and its chemical composition (in wt.%) is shown in Table 1. This data was first published by Stratford [16].

Experimental creep punch tests were conducted on both 0.5Cr–0.5Mo–0.25V and 1.25Cr–0.5Mo steel in a argon environment. The 0.5Cr–0.5Mo–0.25V discs were cut from the same virgin material described above. In total, 15 discs with 9.0 mm diameter and a thickness of 0.5 mm were then cut from the virgin material. (Note this disc thickness is as recommended by CEN, but the diameter is closer to that recommended by the analysis of the numerical modelling results.) These discs were then tested at a single temperature of 848 K but over a load range of 170–420 N. The 1.25Cr–0.5Mo steel material described above was first uniaxially tested at 848 K and at a constant load of 135 MPa. Under these conditions the material has a life of around 536 h, but the specimen was removed from test after 300 h (approximately three times the minimum creep rate). Ten discs with 9.0 mm diameter and a thickness of 0.5 mm were then cut from the tested specimen. This pre-damaged steel was then punch tested at temperatures of 848 and 903 K and over a load range of 170–300 N. The experimental rig (see Fig. 1 for details) used a disc diameter of 9.0 mm and a disc thickness of 0.5 mm. It had a punch radius of 1.0 mm and a punch hole radius of 4.0 mm. No attempt was made to lubricate specimens and the disc edges were rigidly clamped.

During all small punch creep tests described above, measurements were made of punch displacement (in millimetre) through time (in seconds) so that complete displacement–time curves were derived. Displacement rates (in millimetre/second) were then found by numerically differentiating this displacement–time data and

minimum displacement rates found by smoothing through these displacement rates.

Finite element modelling of the small punch test

Figure 1 shows the punch test at some point where the punch has been displaced a distance d. The initial disc had a diameter x_2 and thickness x_3, the hemispherical punch has a radius x_4 and the punch hole a diameter x_1. An axial load $F(= x_7)$ is applied to the rear of the punch and this results in deformation of the specimen disc (ABCDEFG are points on the disc surface). Deformation is assumed to be visco-plastic and at constant volume with deformation rates being governed by the creep properties of the material. The driving force for deformation is F but the disc sees this through the interface AB(area $= \Omega^{AB}$). There are frictional forces along Ω^{AB} and therefore the distribution of normal and shear tractions are not known a priori. Frictional forces will be described by the constant shear rule,

$$k = x_5 \frac{\bar{\tau}}{\sqrt{3}} \tag{1}$$

where $0 \leq x_5 \leq 1$ and $\bar{\tau}$ is the local Von Mises flow stress. The disc surface area CDEF is either clamped to prevent any relative movement or unclamped. Clamped is taken to mean that points on the disc surface adjacent to CD and FE are restrained from movement in both the r and z direction. Unclamped means that the same surface points are restrained only in the direction of z. Figure 1 represents the test at one instant and changes in the geometry occur with time as punch penetration proceeds. Measured outputs from the test are the displacement of the punch, d, as a function of time, the time to rupture and the displacement to rupture. From this minimum displacement rates are easily calculated.

At any disc configuration and neglecting body forces the equilibrium equations are

$$\tau_{ij,j} = 0 \tag{2}$$

where τ_{ij} is the Cauchy stress tensor. For any arbitrary perturbation of the velocity field u_i

$$\int_V \tau_{ij,j} \delta u_i \, dV = 0 \tag{3}$$

and from the divergence theorem, the symmetry of the stress tensor and imposing $\delta u_i = 0$ on essential boundary conditions,

$$\int_V \tau_{ij}\delta\dot{\xi}_{ij}\,\mathrm{d}V - \int_{\Omega^{AB}} F_i\delta u_i\,\mathrm{d}\Omega^{AB} - \int_{\Omega^{CF}} F_i\delta u_i\,\mathrm{d}\Omega^{CF} = 0 \tag{4}$$

F_i are the local surface tractions at u_i and $\dot{\xi}_{ij}$ is the strain rate tensor. For incompressible deformation

$$\int_V \tau'_{ij}\delta\dot{\xi}_{ij}\,\mathrm{d}V + \int_V \tau_m\delta\dot{\xi}_{ii}\,\mathrm{d}V$$
$$- \int_{\Omega^{AB}} F_i\delta u_i\,\mathrm{d}\Omega^{AB} - \int_{\Omega^{CF}} F_i\delta u_i\,d\Omega^{CF} = 0 \tag{5}$$

where τ'_{ij} is the deviatoric stress and τ_m the mean stress, subject to the constraint

$$\int_V \dot{\varepsilon}_{ii}\,\mathrm{d}V = 0 \tag{6}$$

For the quasi-static situation of Fig. 1, Eq. 5 has been solved by finite element methods and full details have been given elsewhere [11] together with examples of the meshes used and typical graphical outputs from the programme. The equation has been discretised with eight nodded isoparametric quadrilateral elements with the constraint of Eq. 6 applied by a penalty function procedure. Equation 5 and its discretised form are non-linear so that the solution for the admissible velocity field must be approached iteratively. Furthermore, the values of F_i are not known so that further iteration is required to ensure that the total punch load is equal to F. The iterative algorithm is given in [11]. The whole problem is also geometrically non-linear and after each stable iteration nodal coordinates are updated by a one-step Euler algorithm. The updating also keeps account of punch displacement as a function of time and of the current values of the internal variables in the constitutive equation including the accumulation of creep damage.

The high temperature creep properties used in the model have been derived from extensive uniaxial and biaxial creep testing of 0.5Cr–0.5Mo–0.25V and 1.25Cr–0.5Mo steels at 565 °C [19, 20]. These multi-axial stress tests have confirmed that the material behaves as a Von–Mises solid (i.e. the Levy–Mises flow rule is obeyed). The general constitutive relationship relating strain rate to current material conditions has been derived as a phenomenological internal variable model [13]. The basic rate equation includes work hardening, thermal softening and creep damage as internal variables and includes subsidiary equations which govern the growth of these variables in the creep situation [11]. In particular, the growth of creep damage during the punch test can be followed.

While, for virgin material, the internal variables are initially set to zero, this is not a necessary condition so that the model can be run with any preexisting continuum damage. Thus damage can be regarded as an independent variable when running the model and simulations for materials with preexisting damage are possible. Damage has been assigned the variable x_6. The creep experiments have shown that fracture occurs when the accumulated damage reaches a critical value [13, 20]. This value has been shown to be a function of the current stress tensor and this forms the basis of a fracture criterion which has been incorporated in the punch test model. More specifically, at a given load and temperature, the accumulated damage at failure is given by

$$W_{\mathrm{crit}} = \frac{1}{\theta_3}\left[\varepsilon_f - \theta_1\left(1 - e^{-\theta_2 t_f}\right)\right] \tag{7a}$$

where t_f is the time at failure, ε_f is elongation at failure and θ_1 to θ_3 are the theta values used to describe the creep curve for 0.5Cr–0.5Mo–0.25V and 1.25Cr–0.5Mo steels at such a given load and temperature

$$\varepsilon_t = \theta_1\left(1 - e^{-\theta_2 t}\right) + \theta_3(e^{\theta_4 t} + 1) \tag{7b}$$

where ε_t is the strain at time t. To calculate a value for W_{crit}, the punch test model obtains θ_j ($j = 1,\ 4$) and ε_f values at any stress or temperature using the following empirical relations

$$\ln\theta_j = a_{j,0} + b_{j,0}\sigma + c_{j,0}T + d_{j,0}\sigma T \quad j = 1, 4 \tag{8a}$$

$$\ln\varepsilon_f = a + b\sigma + cT + d\sigma T \tag{8b}$$

where T is temperature and σ is stress. The failure time t_f (defined as the time to reach the failure strain) is obtained by numerically solving

$$\varepsilon_f = \theta_1\left(1 - e^{-\theta_2 t_f}\right) + \theta_3\left(e^{\theta_i t_f} + 1\right) \tag{8c}$$

These theta values, and the parameters in Eqs. 8, have been published extensively and can be found, for example, in Evans and Wilshire [21]. The value for x_6 in the punch test model can therefore be given a quantity between 0 (corresponding to no preexisting damage) and just below W_{crit} (corresponding to preexisting damage that exists just before failure).

This punch test model can be made stochastic by taking into account the variability in the estimated θ_j values as measured by their variance, γ_j. Consequently, the parameters of Eq. 7b and W_{crit} in Eq. 7a are also subject to uncertainty. The above deterministic model is made stochastic as follows:

1. From a series of multiaxial tests produce estimates of θ_j using the nonlinear optimisation procedure put forward by Evans [22]. Then using the estimated theta values produce estimates for the parameters $a_{j,0}$, $b_{j,0}$, $c_{j,0}$, $d_{j,0}$ of Eq. 8a, and a, b, c, and d of Eq. 8b using the weighted least squares procedure put forward by Evans [22]. This makes Eqs. 8a, b operational. This equation should be interpreted as determining the mean value for Θ_j, $\bar{\Theta}_j$. That is,

$$\bar{\Theta}_j = a_{j,0} + b_{j,0}\sigma + c_{j,0}T + d_{j,0}\sigma_i T \tag{9a}$$

where $\ln(\theta_j) = \Theta_j$.

However, there is no reason to suppose that the variance of each Θ_j will also depend on the test conditions. The natural log of each θ_j is therefore assumed to have the same variance given by the average, over all test conditions, of the individually estimated variances. Call this ρ_j.

2. In the absence of any prior knowledge on theta distributions, each θ_j is assumed to follow a log normal distribution, implying that the $\ln(\theta_j) = \Theta_j$, are normally distributed. Thus, $\ln(\theta_j)$ is taken to be normally distributed with a mean and variance of

$$\ln(\theta_j) \sim N(\bar{\Theta}_j, \rho_j)$$

Values for Θ_j can be drawn from this distribution using

$$\hat{\Theta}_j = \bar{\Theta}_j + \sqrt{\rho_j}\left[\Phi(U)^{-1}\right] \tag{9b}$$

where U is a randomly drawn number between 0 and 1 and $\Phi(U)$ is the cumulative normal density function, i.e. $\Phi(U)^{-1}$ is a standard normal variate. By drawing random values between 0 and 1 for U (four at each of the test conditions), Eq. 9b can be used to obtain simulated values for each Θ_j at each test condition, and therefore $\hat{\theta}_j = \exp(\hat{\Theta}_j)$.

3. Using these simulated values for $\hat{\theta}_j$ the following regressions can be carried out

$$\hat{\Theta}_{j,k} = a_{j,k} + b_{j,k}\sigma + c_{j,k}T + d_{j,k}\sigma_i T \tag{9c}$$

The parameters are again estimated using weighted least squares. $k = 1$ in Eq. 9c.

4. For each of the stresses and temperatures that make-up the test matrix of step 1, the punch test model obtains interpolated values for θ_j, and ε_f by using Eqs. 9c and 8b. t_f is then obtained by solving Eq. 8c using these θ_j and ε_f values. All these are then substituted into Eq. 7a to obtain the simulated value of W_{crit} at each test condition.

5. The empirical relationship between $\ln(W_{crit})$ and σ and T can then be established through use of a simple linear regression. Linear least squares is applied to

$$\ln W_{crit,k} = m_k + f_k \ln \sigma^* \tag{9d}$$

so as to obtain estimates for m_k and f_k, $(k = 1)$ where

$$\sigma^* = \frac{\sigma}{163309 + 127.1T - 0.1419T^2} \tag{9e}$$

6. Select a variety of stress and temperature combinations within the range of conditions defined by the experimental test matrix in step 1. The punch test model is then run at each of these test conditions, using the W_{crit} values obtained from Eqs. 9d and 9e until a failure time is observed (i.e. until $W = W_{crit}$). This produced a complete time–displacement graph for each of the selected test conditions (including the eventual failure time of the disc). From these time–displacement curves minimum displacement rates can be easily calculated.

7. Repeated the above steps $k = 1$ to M times so that M failure time predictions and time–displacement curves are obtained at each of the test conditions selected in step 6. In this article $M = 15$.

Results

Estimated values for θ_j, $a_{j,0}$, $b_{j,0}$, $c_{j,0}$, $d_{j,0}$ a, b, c, d, m and f have been tabulated in a previous paper by Evans and Wang [23] and readers are referred to that paper for further details. All the predictions from the punch test model shown in this article are derived using a friction factor of 0.35 ($x_5 = 0.35$).

Verification results

0.5Cr–0.5M0–0.25V steel was selected for verifying the model under undamaged conditions. Corresponding to step 6 in the above section, Table 2 contains the stresses chosen to run the punch model. At all these stresses the temperature selected was 848 K. Substituting these test conditions into Eqs. 9e and 9d yields predictions for critical damage at these test conditions. The second column of Table 2 contains these predicted W_{crit}. The punch test model was then run using the W_{crit} values shown in Table 2 until failure times were observed (i.e. until $W = W_{Crit,i}$). These predicted failure times are shown in the final column of Table 2.

The above steps were repeated another 14 times to yield $k = 15$ failure time predictions at all the stresses shown in Table 2. All these predictions, in seconds, are shown in Table 3. At the bottom of Table 3 are the averages and standard deviations of the 15 predictions at each test condition. Figure 2 plots these 15 predictions at each stress together with the average predictions at each load. As can be seen, the scatter present in the 15 predictions also appears to increase with decreasing stress. Figure 3 plots the average predictions of Fig. 2 together with bars that depict the range given by these averages plus and minus three of their standard deviations. The experimental punch test results described in the section "The materials" are also superimposed on this graph. It appears that the punch test model is replicating the experimental data very well. All the data appears to be within these approximate 99% confidence intervals and the scatter present in the experimental data match the magnitude of these error bars.

Table 2 Disc modelled failure times as determined by the damage parameters given by Eq. 9d for a temperature of 848 K

Stress (MPa)	W_{crit}	t_f (s)
175	2.4756	3127422
200	2.64356	3127422
225	2.8011	1409683
250	2.9499	629114
275	3.09140	275961
300	3.2265	118580
325	3.3559	49447.6
350	3.4804	20108.5
375	3.6005	7925.84
400	3.7165	3031.13
425	3.8289	1140.5

1.25Cr–0.5Mo steel was selected for verification of the model under damaged conditions. Figure 4a plots the experimental punch test results described in the section "The materials". At each temperature the experimental results suggest that time to failure for these pre-damaged discs varies with stress in a power law fashion. Also superimposed onto the figure are a few punch test results done on undamaged 1.25Cr–0.5Mo steel and the effect of preexisting damage on failure time is easily observed. Figure 4b plots the average predictions made by the punch test model for the load conditions shown in Fig. 4a and at 848 K together with bars that depict the range given by

these averages plus and minus three of their standard deviations. All the data appears to be within these approximate 99% confidence intervals.

The predictions made for both damaged and undamaged materials appear to fully validate the finite element model of the punch test in that nearly all the experimental data falls within the 99% confidence intervals for the models predictions of the experimental data. The model is therefore a realistic description of the small punch creep test when using virgin and damaged material.

Minimum displacement and creep rates

Plots of minimum displacement rate against failure time for the small punch test frequently show the same type of dependency as observed in uniaxial creep tests, but with a shift along the time to failure axis. Figure 5a shows the experimental data obtained on minimum displacement rates (for the small punch test) and minimum creep rates (from preexisting uniaxial tests held at the IRC Swansea) for 0.5Cr–0.5Mo–0.25V steel. The minimum displacement rates are those associated with the experimental failure times in Fig. 3. The source reference for the uniaxial data is [11] and corresponds to the 0.5Cr–0.5Mo–0.25V data set described in the section "The materials". As can be seen, the results do not sit on parallel lines as some other studies have suggested [17]. It is debatable therefore as to whether this similarity or not of the Monkman–Grant type relation

Table 3 Disc modelled failure times associated with 15 runs of the stochastic model

k	Stress (N)										
	175	200	225	250	275	300	325	350	375	400	425
1	3127422	3127422	1409683	629114	275961	118580	49447.6	20108.5	7925.84	3031.13	1140.5
2	2137233	920444	470446	254327	118627	59955.9	28219	12724.3	5180.49	1854.56	599.4
3	5338175	2738739	1393243	682261	316153	137367	55267.1	20820.1	7479.27	2595.49	893.3
4	5540062	2120225	789743	317912	130684	54441.8	22945	8999.76	3783.86	1547.18	607.6
5	3276386	1359214	613599	305172	139585	64818.3	26430.5	11665.1	5069.38	1916.6	702.4
6	7522151	3383550	1511116	662483	281401	115022	44923.4	16597.1	5883.17	1988.48	659.1
7	6968539	2323987	878895	376524	150788	59073	24548.7	9473.5	3775.86	1452.83	605.6
8	6332664	2931486	1370432	652174	300143	127731	51819.2	18497.3	6161.6	2007.38	641.2
9	6644043	2359151	832086	319872	137275	47591.5	18681.6	7913.55	3341	1292.75	487.5
10	11039790	4558597	1871664	756750	298431	114161	42300.1	15116.9	5212.65	1754.83	579.7
11	6.78E+6	3.15E+6	1.45E+6	657772	288198	120504	47874.2	17925.2	6375.1	2197.39	738.78
12	10946190	4277930	1664511	641349	235138	88422.8	33072.7	12411.1	4530.12	1644.99	594.0
13	6202046	2863317	1315426	594658	262242	112127	45776.6	17744.2	6551.93	2333.31	798.0
14	5559516	2829056	1417374	690661	321784	141095	57237.7	21518.4	7601.52	2613.25	873.7
15	8825701	3442292	1339560	517607	199101	75776.6	28607.3	10601.2	3896.9	1413.81	504.8
A	6415840	2825939	1222163	537242	230367	95777.8	38476.7	14807.8	5517.91	1976.27	695.0
S	2551126	955051.5	404836	172009	76028.5	32716.2	12912.0	4566.21	1491.18	499.878	172.0

The shown failure times are in seconds. A is the average of the 15 predicted failure times and S the standard deviation in these failure times
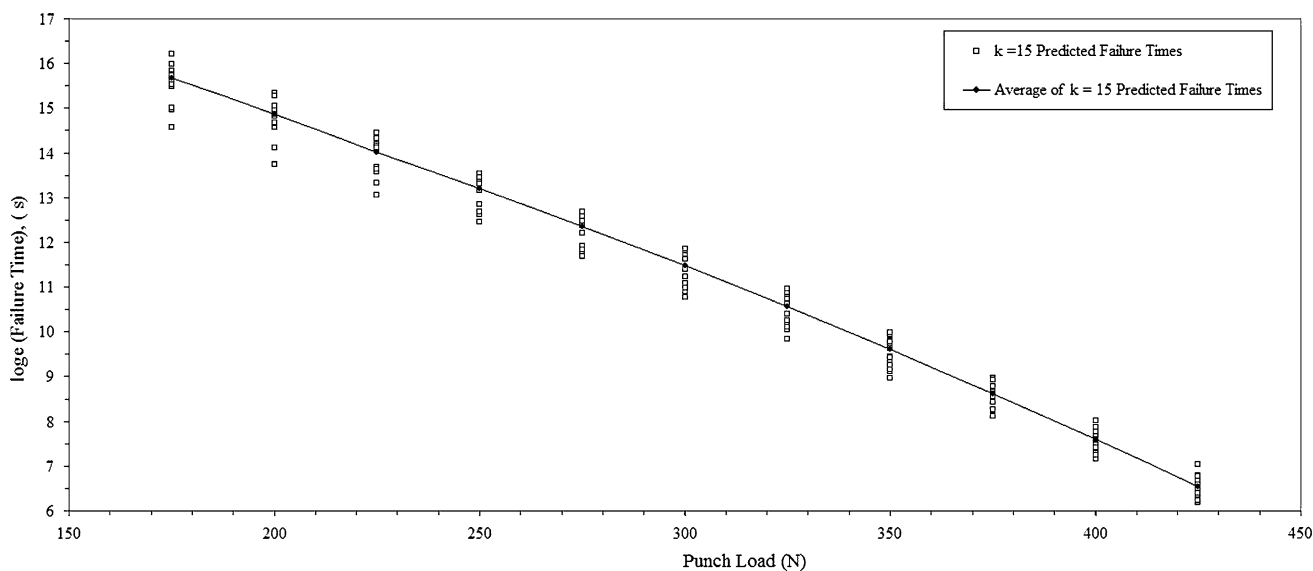
Fig. 2 The $k = 15$ disc modelled failure times at 848 K using virgin 0.5Cr–0.5Mo–0.25V steel

is an intrinsic property of the small punch test or is due to the expected scatter in both uniaxial and more especially small punch test results.

An important objective of this article was to develop a better understanding of this shift, its dependence on test conditions and whether it is always parallel in nature. The punch test model was therefore run 15 times over a wide range of loads with a disc diameter of 9.0 mm, disc thickness of 0.5 mm, punch radius of 1.0 mm and a punch hole radius of 4.0 mm. The resulting 15 slope estimates of the Monkman–Grant type relation are shown in Fig. 5b, together with their average and the models prediction of the 95% confidence interval for this slope. Also shown is the

slope estimated from the uniaxial experimental data in Fig. 5a together with its 95% interval.

Having taken into account creep variability, the results from the punch test model suggest that the slope of the Monkman–Grant type relation is the same in uniaxial as it is in small punch test data—as revealed by the overlapping intervals. The model therefore predicts identical slopes within the intrinsic variability, so that there is not a statistically significant difference between the two slopes at the 5% significance level. This parallel nature suggests that it will be possible, from the outcomes of future research, to convert small punch test data into uniaxial data using simple analytical expressions.
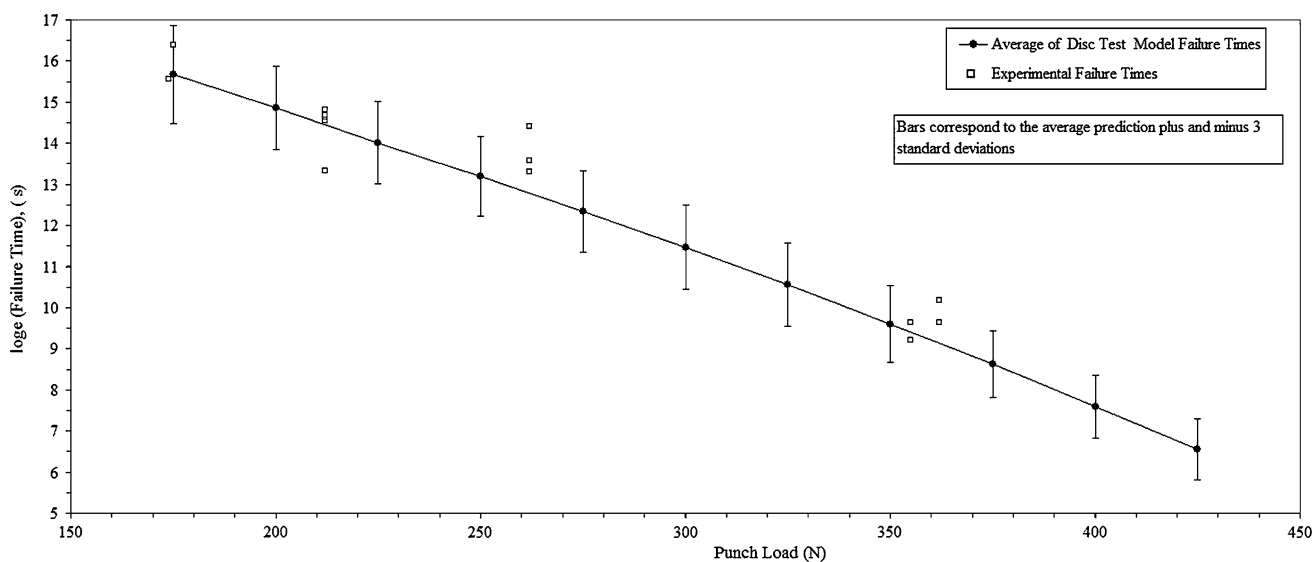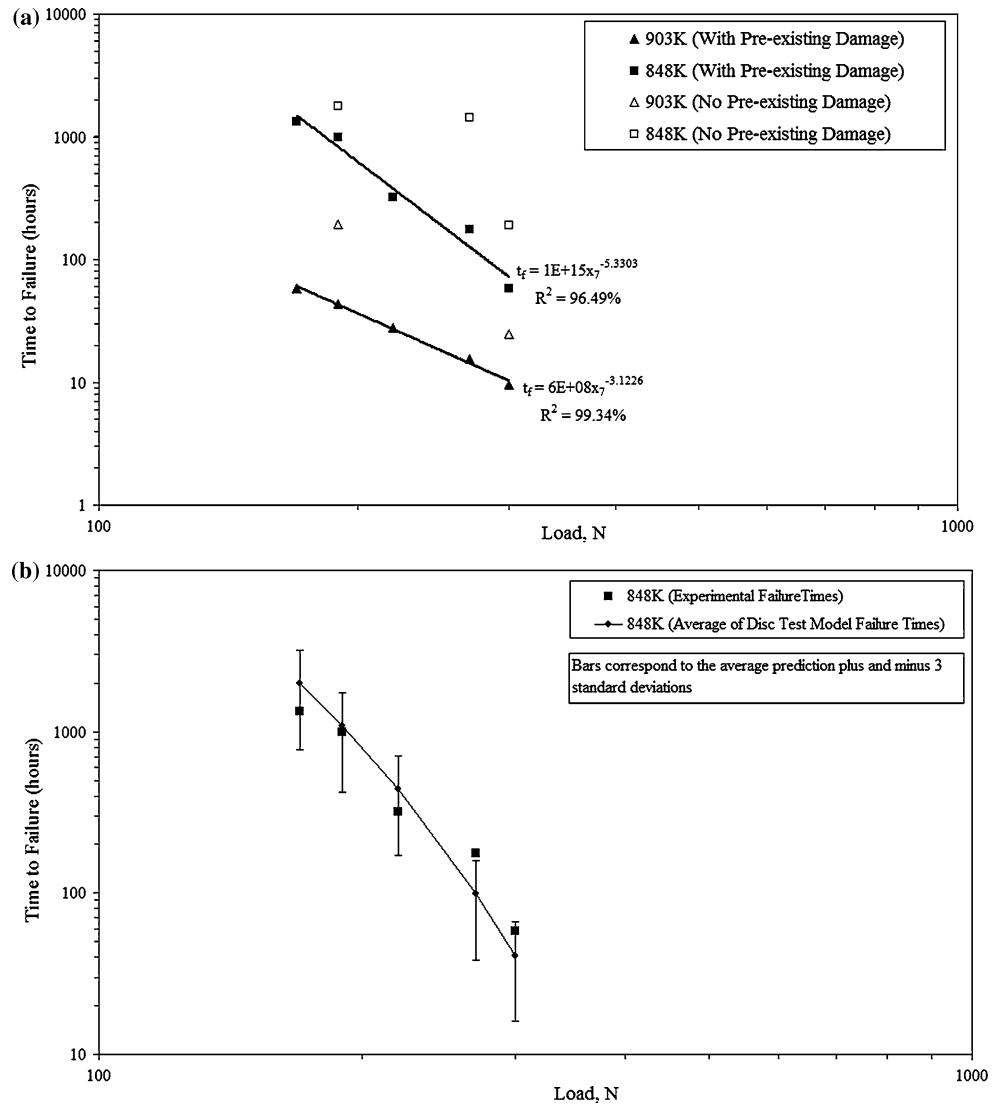

Fig. 3 Failure times from experimental punch tests together with the modelled predictions at 848 K for virgin 0.5Cr–0.5Mo–0.25V steel

Fig. 4 (a) Failure times from experimental punch tests for damaged and virgin 1.25Cr–0.5Mo steel. (b) Failure times from experimental punch tests together with the modelled predictions at 848 K for damaged 1.25Cr–0.5Mo steel

A number of possible avenues suggest themselves. By comparing the model's failure time predictions for varies loads at the optimal test and specimen geometries identified by Evans and Wang [12] with the experimental uniaxial failure times at varies accelerated stresses (both at a given temperature), it should be possible to derive an equation giving the stress corresponding to a particular punch load—$F = f(\sigma)$. (As a lot of short-term uniaxial data is already available, so this presents no additional experimentation). Using this relation the model can be run at the load corresponding to operating stresses and the time to failure recorded. Alternatively, a disc can be cut from an in-service component and put on test at a load corresponding to the operating stress until the minimum creep rate is observed (the test can then be discontinued). This rate can then be inserted into the Monkman–Grant relation implied by the small punch test model to predict when the disc will fail. This procedure will work because, as shown

by Evans and Wang [23], the Monkman–Grant relation predicted by the model is the same at all levels of preexisting damage. Then a parallel adjustment to this failure time will give a prediction of the components remaining life.

Conclusions

The small punch test is an innovative technique based on miniaturised specimens and is a promising solution to the problem of undermining the structural integrity of operating components through the extraction of large test samples. It was found that this model was capable of producing accurate predictions of disc life for disc samples cut from virgin 0.5Cr–0.5Mo–0.25V and damaged 1.25Cr–0.5Mo steel. For both materials it was found that the average predictions from the model at each test condition were in broad
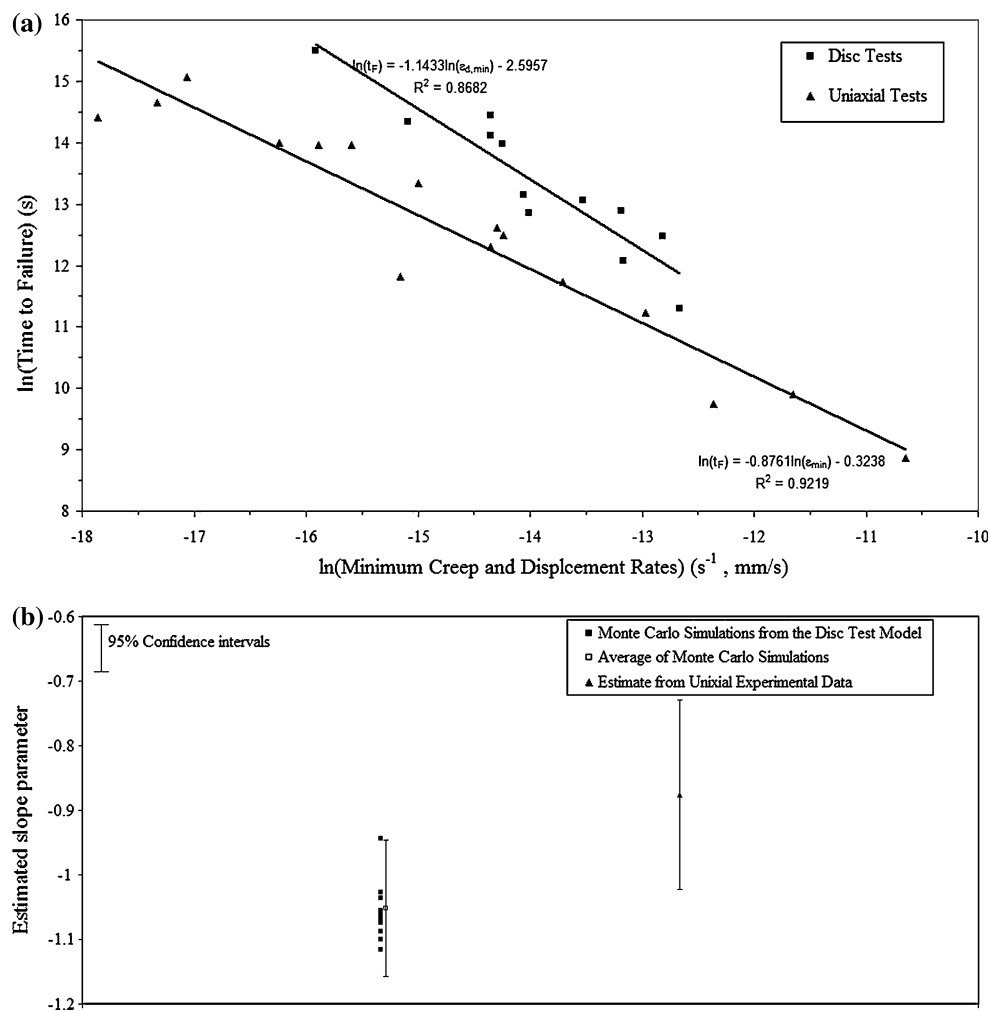
Fig. 5 (a) Monkman–Grant type relations in uniaxial and small punch testing of 0.5Cr–0.5Mo–0.25V steel. (b) Slope parameter of the Monkman–Grant type relation from experimentation and computer modelling of virgin 0.5Cr–0.5Mo–0.25V steel

agreement with the experimental data and that all the data appeared to be within the approximate 95% confidence intervals for these predictions. Having taken into account creep variability in this verified model, displacement rate results from the punch test model suggest that the slope of the Monkman–Grant type relation is the same in uniaxial as it is in small punch test data. The next step is to use the numerical model to identify precisely the nature of the small punch—uniaxial test correlation.

References

1. Manahan MP, Argon AS, Harling OK (1981) J Nucl Mater 103–104:1545. North-Holland Publishing Company
2. Mao X, Takahashi H (1987) J Nucl Mater 150:42. North-Holland
3. Takahashi H, Shoji T, Mao X, Hamaguchi Y, Misawa T, Saito M, Oku T, Kodaira T, Fukaya K, Nishi H, Suzuki M (1988) Recommended practice for small punch (SP) testing of matallic materials. JAERI-M 88-172, Sept
4. Foulds JR, Jewitt CW, Bisbee LH, Whicker GA, Viswanathan R (1992) Miniature sample removal and small punch testing for in-service component FATT. Proceedings, Robert I. Jaffee memorial symposium on clean materials technology ASM, pp 101–109
5. Parker JD, Stratford GC, Shaw N, Spink G, Tate E (1995) Deformation and fracture processes in miniature disc tests of CrMoV rotor steel. Proceedings, third international Charles Parsons turbine conference, vol 2. Institute of Materials, pp 418–428
6. Bicego V, Lucon E, Crudeli R (1995) Integrated technologies for life assessment of primary power plant components. In: Bicego, Nitta, Viswanathan (eds) Proceedings of int. symp. on materials ageing and component life extension, vol I. EMAS, pp 295–305
7. Bulloch JH, Fairman A (1995) Some considerations regarding the small punch testing of important engineering components. In: Hietanen, Auerkari (eds) Proceedings of int. conf. Baltica III, Helsinki, Stockholm, 6–8 June 1995, pp 179–193
8. CEN Workshop Business Plan (2004) Small punch test method for metallic materials. CEN, Brussels, Belgium, Sept 2004
9. Bicego V, Rantala H, Klaput J, Stratford GC, Persio F, Hurst RC (2004) The small punch test method: results from a European creep testing round robin. Proceedings, EPRI conference on life assessment, Hilton Head Island

10. CEN Workshop Agreement (2006) CWA 15627:2006 E, Small punch test method for metallic materials. CEN, Brussels, Belgium, Dec 2006

11. Evans RW, Evans M (2006) J Mater Sci Technol 22(10):1155

12. Evans M, Wang D (2007) Mater Sci Technol 23:883

13. Evans RW (2000) Proc R Soc Lond A 456:835

14. Hankin GL, Toloczko MB, Johnson KI, Khaleel MA, Hamilton ML, Garner FA, Davies RW, Faulkner RG. An investigation into the origin and nature of the slope and the x-axis intercept of the shear punch-tensile yield strength correlation using finite element analysis. In: Hamilton ML et al (eds) Effect of Irradiation on material, 19th international symposium. ASTM 1366, p 1018

15. Evans M, Wang D (2007) J Strain Anal Eng Des 5:389

16. Stratford GC, Di Persio F, Klaput J (2005) Miniaturised creep testing using the small punch test technique. In: 11th international conference on fracture, Turin, Mar, p 4175

17. Aide Memoire (2006) Miniaturised testing: micro structural evaluation and residual lifetimes. In: The special interest group meeting. National Physical Laboratory, Teddington, 14 Feb 2006

18. Evans RW, Beden I, Wilshire B (1984) Creep life prediction for 0.5Cr 0.5 Mo 0.25 V ferretic steel. In: Wilshire B, Owen DRJ (eds) 2nd international conference on creep and fracture of engineering materials and structures. Pineridge Press, Swansea, p 1277

19. Stratford GC (1994) Type IV cracking in 1 1/4Cr-0.5Mo low alloy steel welds. Ph.D. thesis, University of Wales, Swansea

20. Evans RW, Wilshire B (1996) Constitutive laws for high temperature creep and fracture. In: Krausz AS, Krausz K (eds) Unified laws of plastic deformation. Academic Press, London, pp 107–152

21. Evans RW, Wilshire B (1993) An introduction to creep, 2nd edn. Institute of Materials, London

22. Evans RW (1989) Mater Sci Technol 5:699

23. Evans M, Wang D (2007) Mater Sci Technol 23(8):883